


Seismo-acoustic coupling in the deep atmosphere of Venus

Gil Averbuch,^{1,a)}  Reyna Houston,² and Andi Petculescu²

¹*Southern Methodist University, Roy M. Huffington Department of Earth Sciences, Dallas, Texas, USA*

²*University of Louisiana, Department of Physics, Lafayette, Louisiana, USA*

ABSTRACT:

The extreme conditions at the surface of Venus pose a challenge for monitoring the planet's seismic activity using long-duration landed probes. One alternative is using balloon-based sensors to detect venusquakes from the atmosphere. This study aims to assess the efficiency with which seismic motion is coupled as atmospheric acoustic waves across Venus's surface. It is, therefore, restricted to the immediate neighborhood of the crust-atmosphere interface. In order to account for supercritical conditions near the surface, the Peng-Robinson equation of state is used to obtain the acoustic sound speed and attenuation coefficient in the lower atmosphere. The energy transported across the surface from deep and shallow sources is shown to be a few orders of magnitude larger than on Earth, pointing to a better seismo-acoustic coupling. For a more realistic scenario, simulations were made of the acoustic field generated in the lower atmosphere by the ground motion arising from a vertical array of subsurface point-force sources. The resulting transmission loss maps show a strong epicentral cone accompanied by contributions from leaky surface waves. Results at 0.1 Hz and 1 Hz confirm that the width of the epicentral cone is larger at lower frequencies.

© 2023 Acoustical Society of America. <https://doi.org/10.1121/10.0017428>

(Received 15 July 2022; revised 31 December 2022; accepted 12 February 2023; published online 20 March 2023)

[Editor: Olga Umnova]

Pages: 1802–1810

I. INTRODUCTION

Since the first successful attempts to measure Venus's electromagnetic reflectivity in the 1950s and 1960s (Pettengill and Price, 1961; Smith, 1963; Victor and Stevens, 1961), radar observations—at first from ground stations, then also from spacecraft—have been used to observe the Venusian environment. It was not until the Magellan mission (1989–1994) that Venus's entire surface was mapped at a higher resolution than any other missions or Earth-based observations. From the Magellan data, Venus seems to have various landscape regions that display large-scale compressional and extensional deformation (Leftwich *et al.*, 1999), as well as evidence of possible faulting (Solomon *et al.*, 1991).

Simulations suggest that Venus has a brittle upper crust and upper mantle, similar to Earth (Byrne *et al.*, 2021; Zuber, 1987). While Venus's surface experiences extreme temperatures, there is evidence of brittle deformation, as seen in areas such as Lavinia Planitia (Byrne *et al.*, 2021) and Hippolyta Linea (Solomon *et al.*, 1991). Furthermore, the presence of volcanic materials and evidence of lava flows indicate volcanic events, which may be as frequent as 20 events in 60 days (Byrne and Krishnamoorthy, 2022). These arguments support the hypothesis that Venus is seismically active.

Analyzing Magellan radar data to investigate formations near highly deformed areas (*tesserae*) as well as evidence of stress accumulated around lowlands, the hypothesis has been made that the Venusian surface may be fractured in small

“blocks” in jostling motion somewhat similar to that of ice floes (Byrne *et al.*, 2017; Byrne *et al.*, 2018; Byrne *et al.*, 2021). Nevertheless, given the sparse direct measurements, Venus's internal structure and its dynamics continue to be an open question. Seismic data from the planet can aid in the advancement of this knowledge. Venus has a harsh surface environment with extreme temperature and pressure, making it challenging to develop landing probes. One viable alternative is using high-altitude balloon-based sensors to detect the infrasound signals generated by seismic activity. The sensors can be microbarometers that measure pressure fluctuations (Bowman *et al.*, 2022; Krishnamoorthy *et al.*, 2019) or temperature sensors that could record the temperature fluctuations accompanying acoustic propagation (Garcia *et al.*, 2005). Experiments to detect earthquakes using high-altitude balloons have been successfully completed by Brissaud *et al.* (2021).

Measurements from the Venera 7–14, VeGa-2, and Pioneer Venus Multiprobe landers and descent probes provided the first *in situ* measurements of Venus's atmosphere. The pressure at the surface of Venus is ~90 bar, and the temperature is ~730 K, which is well above the critical values for CO₂ and N₂ (the main atmospheric constituents). Therefore, the first few kilometers of the Venusian atmosphere are probably in a supercritical state.

The VeGa-2 lander obtained the only reliable information on the atmospheric structure below 12 km. Recently, Lebonnois and Schubert (2017) revisited the VeGa-2 temperature profile, noting that it may defy established paradigms by the apparent lack of a well-mixed layer of constant potential temperature. Specifically, using the VeGa-2 descent measurements of temperature and pressure, combined with CO₂

^{a)}Present address: Woods Hole Oceanographic Institution, Falmouth, MA 02543, USA. Electronic mail: gil.verbuch@whoi.edu

and N_2 concentration profiles, the potential temperature profile was obtained; it has a pronounced negative gradient over the first 7 km from the surface, indicating a rather large convective (unstable) layer, followed by a stable layer of increasing potential temperature up to about 17 km. This structure is atypical for a planetary boundary layer because it lacks a dominant well-mixed region.

Lebonnois and Schubert (2017) hypothesize that the density difference between N_2 and CO_2 could lead to a separation of the two species near the surface, possibly by density-driven convection or molecular diffusion; the N_2 mole fraction from $\sim 3.5\%$ at 7 km to $\sim 0\%$ at the surface produces a fairly constant potential temperature over the first 7 km, indicative of convective instability. However, recent numerical simulations of turbulent mixing in Venus's lower atmosphere indicate that chemical species separation is unlikely (Morellina and Bellan, 2022). Nevertheless, whether density-driven separation occurs or not, the atmospheric specification in the supercritical layer needs to be addressed in more detail. For example, the potential temperature profile should be obtained by calculating enthalpy changes with a real-gas equation of state such as the Peng-Robinson equation of state (P-R EoS) instead of the usual ideal-gas framework.

The ability to detect venusquakes from aerial platforms and study its subsurface relies on the efficiency with which ground motion couples to the planet's deep atmosphere through acoustic waves. This article aims to assess the seismo-acoustic coupling strength at the surface of Venus. Its scope, therefore, is limited to the planet's lowermost atmosphere, which is believed to be in a supercritical state. The results presented here are a necessary stepping stone for future studies investigating infrasonic arrivals from venusquakes to high-altitude balloon-borne sensors. In Sec. II, we present the vertical profiles of the sound speed and attenuation coefficient at 1 Hz in the Venusian lower atmosphere. They are obtained using the P-R EoS, appropriate for supercritical conditions. Section III describes the transfer of acoustic energy from deep

and shallow sources across the surface. Plane-wave reflection and transmission coefficients are calculated and compared to their Earth counterparts, as well as the apparent enhancement of power flow from shallow sources (i.e., within a wavelength from the interface). Section IV shows seismo-acoustic simulation results of acoustic propagation from underground sources; the simulations are done in the frequency-wavenumber space, with underground sources placed at various depths. The Appendixes contain details on implementing the P-R EoS in the Venus wavenumber model, as well as the calculations of plane wave reflection and transmission coefficients and spherical-wave power flux from a shallow source. Finally, in Sec. V, we summarize the principal aspects of the paper and lay out the framework for future studies of the seismo-acoustic coupling mechanisms on Venus.

II. DEEP-ATMOSPHERE SOUND SPEED AND ATTENUATION

In a previous study of the acoustic characteristics of Venus's atmosphere, Petculescu (2016) obtained the attenuation coefficient and acoustic phase speed as functions of altitude and frequency based on the Van der Waals equation of state (VdW EoS). The VdW EoS had been tested successfully a few years before on sound speed data obtained during the Huygens probe's descent on Titan (Petculescu and Achi, 2012). Here, we modify the Venus wavenumber model to accommodate the P-R EoS, which is more appropriate than the VdW EoS for the supercritical conditions of the planet's deep atmosphere. The implementation of the P-R EoS into the Venus wavenumber model is described in the Appendixes. Figure 1 compares both models, i.e., P-R and VdW EoSs; one can see that the difference between the acoustic wavenumbers obtained with the two equations of state becomes smaller with increasing altitude as the atmosphere becomes less dense. Specifically, the difference between the implementation of the two equations of state is that the near-surface sound speed and

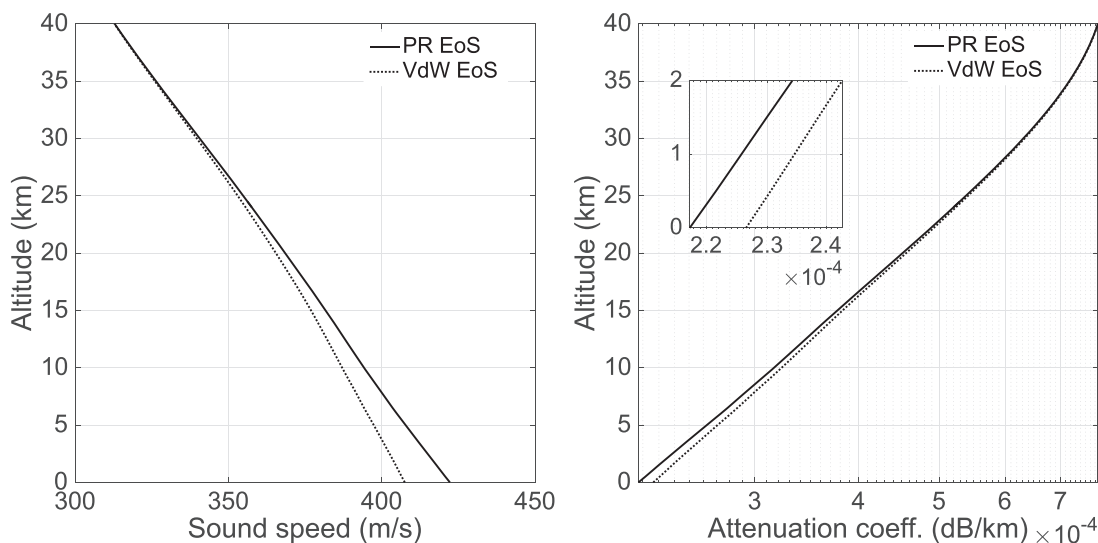


FIG. 1. Vertical profiles of the sound speed and attenuation coefficient at 1 Hz: Van der Waals vs Peng-Robinson EoS predictions. Inset on the right: zoom-in on the attenuation coefficients over the first 2 km.

TABLE I. Elastic and acoustic properties. ρ_0 is the atmosphere’s density (gas), ρ_1 is the crustal density (solid), and λ and μ are the Lamé parameters of the crust. c_0 is the speed of sound in the near-surface atmosphere, and c_L and c_T correspond to P - and SV -wave velocities, respectively.

| | Earth | Venus |
|-------------------------------|--------|--------|
| ρ_0 (kg/m ³) | 1.00 | 68.7 |
| ρ_1 (kg/m ³) | 2700 | 2900 |
| λ (GPa) | 45.7 | 56.4 |
| μ (GPa) | 36.5 | 35.8 |
| c_0 (m/s) | 330 | 422.17 |
| c_L (m/s) | 6629.5 | 6643.6 |
| c_T (m/s) | 3676.8 | 3513.5 |

attenuation coefficient obtained with the P-R EoS are $\sim 3.6\%$ larger and $\sim 4\%$ smaller, respectively, than those obtained using the Van der Waals EoS. In addition, the sound speed profile calculated here with the P-R EoS agrees with that published independently by Morellina *et al.* (2020), who did not address sound absorption. The difference between the acoustic wavenumbers obtained with the two equations of state becomes smaller with increasing altitude as the atmosphere becomes less dense.

III. TRANSMISSION FROM DEEP AND SHALLOW SOURCES

For simplicity, Venus’s crust and near-surface atmosphere are considered homogeneous solid and gaseous media, respectively. Table I gives the atmospheric and mean crustal parameters used as inputs to calculate the energy transmission across the interface in this section.

The Venusian atmospheric density ρ_0 and speed of sound c_0 were computed using the Venus acoustic wavenumber model described in Sec. II. The longitudinal (c_L) and transverse (c_T) velocities are the mean values of the

Lamé parameters and mean crustal density estimated by Yoder (1995) and Yang *et al.* (2016). These values, recently suggested by Xiao *et al.* (2021), are for a basaltic crust (Taylor and McLennan, 2008) and will be considered homogeneous.

We first consider a deep source in a homogeneous semi-infinite solid medium (i.e., many wavelengths below the interface). Therefore, the wavefronts reaching the solid-gas interface are assumed to be plane. The wave polarization can be longitudinal (P waves) or transverse (S -waves). For the latter, we only consider the vertically polarized ones (SV waves) since horizontal polarization cannot be coupled acoustically to the gas. The two wave types are indexed by subscripts L and T , and their incidence angles are denoted θ_L and θ_T . For either incident wave type, the reflected field contains both P and SV waves, while the transmitted field (in the gas) only contains P waves. The seismo-acoustic transfer of energy from the crust into the atmosphere is expressed through the intensity reflection and transmission coefficients, R and T , respectively. Details about their calculation are given in the Appendixes.

Figures 2 and 3 show, respectively, the reflection and transmission coefficients for plane waves at Venus’s surface compared to their Earth counterparts. Solid lines indicate mode preservation (R_{LL} , R_{TT} , T_{LL}), while dashed lines indicate mode conversion (R_{LT} , R_{TL} , T_{TL}); the first index represents the incident mode while the second index shows the transformed mode. Even though the objective of this study is acoustic energy transmission in the atmosphere, showing both the reflection and transmission coefficients is useful because they illustrate energy conservation across the interface through $R_{LL} + R_{LT} + T_{LL} = 1$ (for incident P waves) and $R_{TL} + R_{TT} + T_{TL} = 1$ (for incident SV waves). Both P and SV waves incident from the crust undergo reflection at the interface into both modes. Figure 2 shows a relatively small difference between the calculated reflected values for Earth and Venus; this is because the amount of reflected

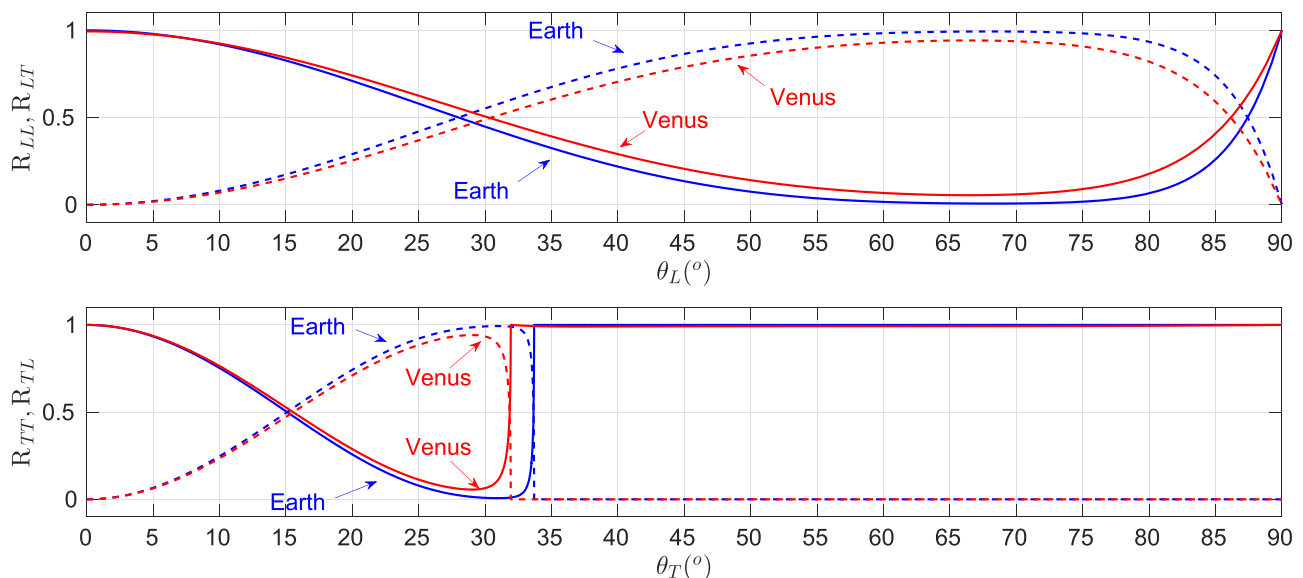


FIG. 2. (Color online) Intensity reflection coefficients for waves incident from the crust into the atmosphere. Top: incident P wave reflected into P wave (R_{LL} , solid) and into SV wave (R_{LT} , dashed). Bottom: incident SV wave reflected into SV wave (R_{TT} , solid) and into P wave (R_{TL} , dashed).

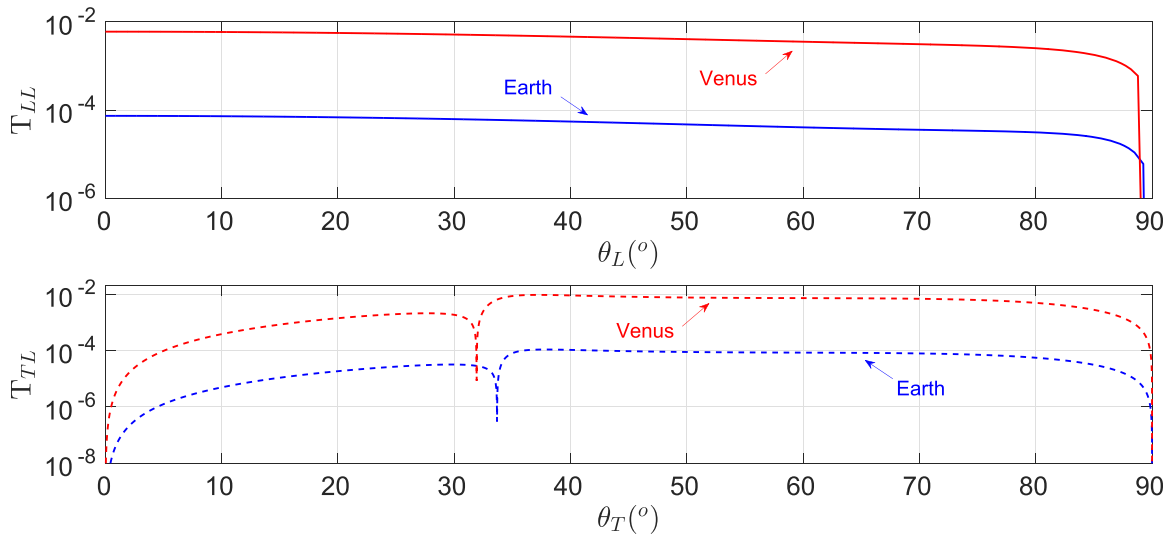


FIG. 3. (Color online) Intensity transmission coefficients for waves incident from the crust into the atmosphere. Top: incident P wave refracted into P wave (T_{LL}). Bottom: incident SV wave refracted into P wave (T_{TL} ; no shear modes in the atmosphere).

energy does not depend on the gas-solid density ratio (although containing the gas density). However, the transmitted energy is proportional to the atmospheric density (see the [Appendixes](#)), which leads to considerably stronger transmission on Venus than on Earth, as can be seen in Fig. 3.

Upon refraction, P waves are coupled into the atmosphere without mode conversion (solid lines), while SV waves suffer mode conversion into P waves (dashed lines). Over the entire range of the incident angle θ_L , the energy transmission coefficient for Venus is two orders of magnitude larger than on Earth; this lies at the heart of the argument that supports Venus’s good seismo-acoustic coupling efficiency. For incident SV waves, the critical angle is $\theta_T^{\text{crit}} \approx 32^\circ$ for Venus and 33° for Earth. Below θ_T^{crit} , most SV -wave energy is reflected, predominantly without mode conversion for $0 < \theta_T < 15^\circ$ and $\theta_T > \theta_T^{\text{crit}}$, and predominantly with mode conversion for $15^\circ < \theta_T < \theta_T^{\text{crit}}$. Beyond the critical angle, the fraction of energy transmitted into Venus’s atmosphere goes through a maximum of $\approx 1\%$ at $\theta_T \approx 37^\circ$ after which it is $\approx 0.75\%$ up to 70° , still several orders of magnitude larger than for Earth.

A seismic source is considered shallow when its distance from the interface is comparable to or smaller than the acoustic wavelength. Then, it can be shown that the power transferred across the interface can be enhanced to the point that it can exceed the power emitted in free space ([Godin, 2011](#); [McDonald and Calvo, 2007](#)). The time-averaged acoustic energy per unit time and unit area (acoustic Poynting vector) transferred from the crust into the atmosphere is $S_{\text{avg}} = \frac{1}{2} \text{Re}(p^* v) = (2\omega\rho_0)^{-1} \text{Im}(p^* \nabla p)$, where v is the particle velocity. Here, the crust-atmosphere interface is defined by $z=0$ in the xy plane; $z < 0$ below the interface, $z > 0$ above the interface. We consider, for simplicity, a monopole source of P waves in the crust, placed at depth $z = -z_s$. This choice of source, although not necessarily realistic for a quantitative study, is used here because it illustrates the effect of the interface in a simple yet compelling manner.

The acoustic power coupled into the atmosphere through the interface is found by integrating the Poynting vector in the vertical direction over the infinite surface area at $z=0$, i.e., $\Pi_{\text{atm}} = \int \int_{(z=0)} S_{\text{avg}} \cdot \hat{z} dA$. Here, \hat{z} is the unit vector normal to the surface. Normalizing to the total P -wave power $\Pi_{\text{em}} = 2\pi(p_0 r_0)^2 / \rho_1 c_L$ emitted in an infinite homogeneous solid, with p_0, r_0 a reference pressure and distance, respectively ([McDonald and Calvo, 2007](#)), one has (see the [Appendixes](#))

$$\frac{\Pi_{\text{atm}}}{\Pi_{\text{em}}} = \frac{m c_L}{2\pi^2 \omega} \int_0^{\omega/c_0} q \left| \frac{T_{LL}(q)}{\nu_L(q)} \right|^2 e^{-2z_s \nu'_L(q)} dq, \quad (1)$$

where $m \equiv \rho_0/\rho_1$ is the gas/solid density ratio, $T_{LL}(q)$ is the Fourier component of the plane wave displacement-amplitude transmission coefficient, q is the horizontal wavenumber, $\nu_L = (k_L^2 - q^2)^{1/2}$ is the vertical wavenumber, and $\nu'_L \equiv \text{Im}(\nu_L)$.

For a more realistic picture, we account for lossy P and SV waves in the crust via the respective quality factors, Q_L and $Q_T \approx \frac{4}{3} Q_L$. In the literature, these vary greatly depending on the type of wave, the material, experimental conditions, etc. Here, we adopt the values $Q_L = 125$ and $Q_T = 56$ for both planets, based on [Johnston et al. \(1979\)](#), and the wavenumbers are $k_L = \omega c_L^{-1} (1 + i/2Q_L)$ and $k_T = \omega c_T^{-1} (1 + i/2Q_T)$, respectively.

The normalized power coupled into the atmosphere by a shallow omnidirectional P -wave source is shown in Fig. 4 as a function of source depth divided by the wavelength in the source medium (i.e., dimensionless source depth). For deep sources ($z_s/\lambda_L \geq 10^{-1}$), the coupled acoustic power agrees with the plane wave transmission coefficients in Fig. 3 predicting two orders of magnitude higher amplitudes on Venus than on Earth. For decreasing source depths, the acoustic power coupled into the atmosphere at the surface increases to the point where it can exceed the emitted power by more than 30 dB. Furthermore, since the acoustic energy

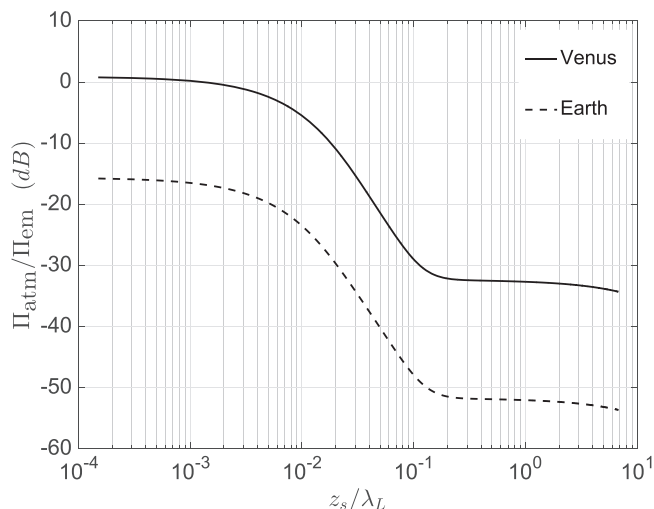


FIG. 4. Normalized power transmitted across the interface from a simple P -wave source in the crust, as a function of dimensionless source depth.

flux through the interface is proportional to the atmospheric density, the effect is amplified on Venus by ~ 15 dB, indicating a more efficient seismo-acoustic coupling. Once generated, the waves will travel in the vertically stratified atmosphere while undergoing losses characterized by the attenuation coefficient such as that shown in Fig. 1. Nevertheless, absorption in the Venusian atmosphere is consistently smaller than in Earth's for frequencies below 100 Hz (Petculescu and Lueptow, 2007).

IV. SEISMO-ACOUSTIC SIMULATIONS

In order to simulate infrasound propagation in Venus's lower atmosphere from an underground source, the seismo-acoustic fast field program is used (Averbuch *et al.*, 2020a; Jensen *et al.*, 2011). It is a frequency-wavenumber (f - k) solver that provides an exact solution for propagation in layered media. The method is based on dividing the medium into piecewise, homogeneous layers while the exact solution of the wave equation describes the wavefield within each layer; imposing the continuity of stress and displacement at the layer boundaries allows the waves to propagate across layers. The specific treatment of the boundary conditions enables propagation through the discontinuous density and velocity profiles of Venus's subsurface and atmosphere.

On Earth, long-range infrasound propagation is facilitated by atmospheric waveguides arising from temperature inversions and wind profiles (Evers and Haak, 2010), which allow efficient propagation of trapped modes over hundreds to thousands of kilometers (Arrowsmith *et al.*, 2021; Averbuch *et al.*, 2020b; Shani-Kadmiel *et al.*, 2021; Waxler *et al.*, 2017). Venus has strong high-altitude zonal winds, with speeds reaching 100 m/s, which may contribute to energy transport radially away from the epicenter. However, based on the current speed of sound profiles, these high-altitude winds may not be strong enough to refract acoustic waves back to the ground. Moreover, for propagation above 20 km, the attenuation of clouds should be considered. Due

to these reasons, propagation to higher altitudes will not be addressed in this study.

For the seismo-acoustic simulation, we use the density and velocity profiles based on the values in Table I and Fig. 1. Due to the uncertainties of Venus's seismicity, vertical lines of 0.1 and 1 Hz *point force sources* are placed in depths ranging from 1 to 10 km. Unlike a monopole, a point force has both longitudinal and transverse components; hence it generates both P and S waves (Ewing, 1957; Madariaga, 2015). Thus, placing a vertical line of point forces leads to a better approximation of a seismic wavefield.

The resulting transmission loss (TL) is shown in Fig. 5 up to an altitude of 20 km. As a function of horizontal range, the relatively high TL values from 0 km downrange to 50 or 100 km (for 1 or 0.1 Hz sources, respectively) can be explained by the efficient coupling of P and SV waves above the source (Fig. 3). The subsequent steady decrease in TL is associated with radiation from the leaky Rayleigh mode. As expected, pressure amplitudes from the 0.1 Hz vertical forces line are several orders of magnitude higher than from the 1 Hz sources. The excess transmitted power compared to Fig. 4 is ascribed to the transverse waves component of the source (Godin, 2011) that was not taken into account in Sec. III. In terms of absolute pressure, these results suggest the following, (1) for the 1 Hz source, the expected pressure above the source ($z = 20$) at $r \leq 100$ km is 100 times larger than at $r = 500$ km; (2) the amplitude ratio at $r = 500$ km and $z = 1$ km is twice as at $z = 20$ km.

The simulation results show that most of the acoustic energy in the lower atmosphere is constrained to a (relatively) narrow cone above the epicenter, the rest being conveyed laterally as radiation from decaying surface waves. The cone's width and the coupled waves' amplitudes are inversely proportional to the frequency, i.e., a lower source frequency leads to a broader cone and higher coupled pressure amplitudes. As can be observed from the difference between the TL vs range plots, the width of the epicentral radiation cone becomes narrower at higher frequencies, as expected. The supercritical state of the Venusian deep atmosphere plays an important role in determining the initial amplitudes of the generated sound field.

V. CONCLUSIONS

The goal of this study is to investigate the seismic-to-acoustic transfer of energy into Venus's deep atmosphere in windless conditions well below the main cloud level. The ability of seismic events to generate acoustic disturbances in the atmosphere is governed by the acoustic impedance ratio between the crust (assumed a homogeneous solid) and the atmosphere. Venus's lower atmospheric conditions create an "acoustically friendly" environment, whose acoustic impedance is almost two orders of magnitude greater than Earth's, into which seismic ground motion can be coupled more efficiently. The deep atmosphere of Venus is modeled as a real gas via the P-R EoS in order to account for the supercritical conditions of its first few kilometers.

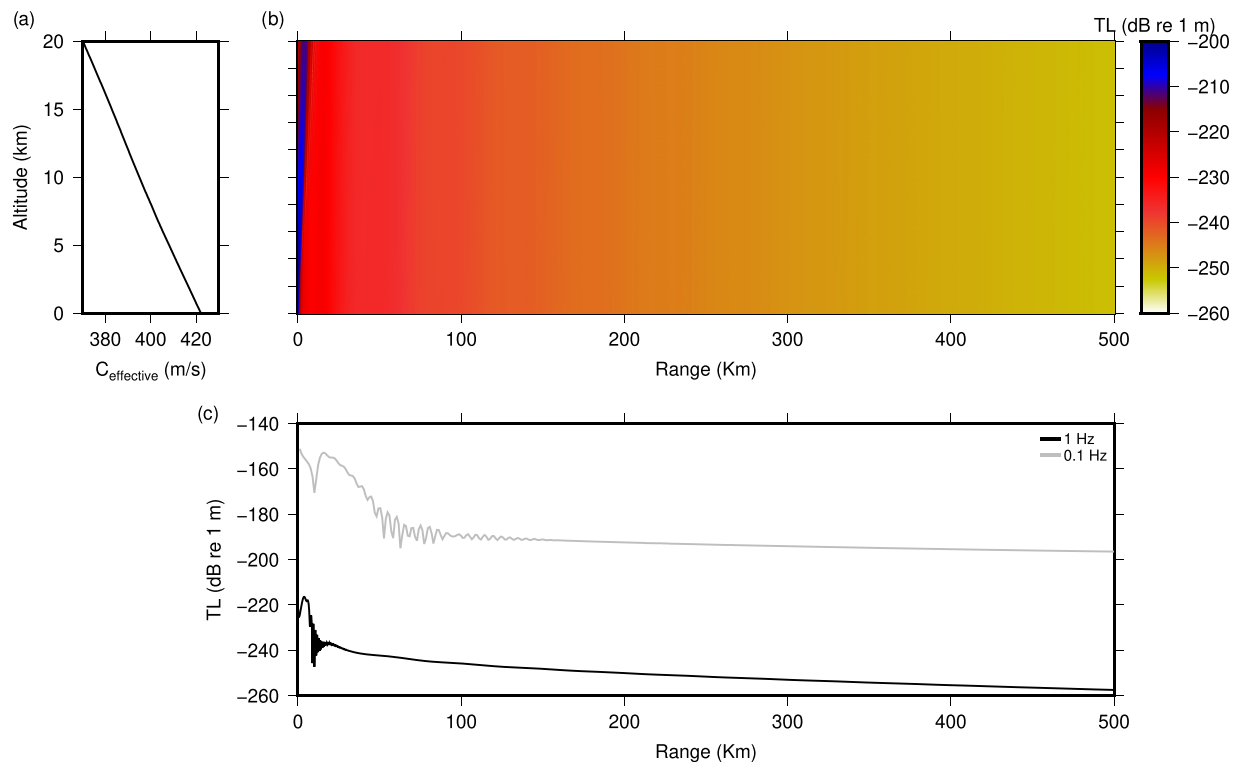


FIG. 5. (Color online) FFP simulation results. (a) Venus effective speed of sound profile; (b) narrowband simulation results at 1 Hz for vertical point-force source array; (c) TL vs range at an altitude of 20 km from a 0.1 and 1 Hz vertical point-force source array.

Characterizing deep sources, plane wave energy transmission across the crust-atmosphere interface is several orders of magnitude stronger than on Earth, over many incidence angles, because of Venus's ~ 70 times lower crust-atmosphere impedance contrast. A seismic source is considered shallow if situated within an acoustic wavelength from the interface. Here, we exemplify with a monopole source of longitudinal waves, placed at depth z beneath the surface such that $z/\lambda_L < 1$, where λ_L is the P -wave wavelength. A considerable amount of acoustic power is transmitted through the interface, in excess of 30 dB compared to deep sources. Moreover, more than 15 dB excess is expected compared to Earth.

Propagation simulations in the lower atmosphere show that the acoustic energy is likely to be concentrated in a relatively narrow cone centered on the epicenter, with some energy leakage from surface waves. The width of the cone, its amplitude, and the leaky surface-wave amplitudes are frequency- and depth-dependent. Furthermore, this study uses a homogeneous elastic half-space; therefore, only one surface wave mode exists. In a more realistic scenario where the subsurface will consist of layered media, more surface wave modes will be excited depending on the source depth and frequency spectrum; the coupling efficiency will change depending on the layers' thickness and elastic properties. Measuring their acoustic manifestation will allow inverting for Venus's sub-surface. The effects of clouds on the acoustic wavenumber [of which preliminary results were reported by Trahan and Petculescu (2020)] as well as the possible emergence of atmospheric waveguides from the interplay between the strong high-altitude

winds and the hot surface are to be addressed in future endeavors.

In the context of the block-tectonics hypothesis, the crust may be fragmented into adjacent blocks held together by frictional stresses. Therefore, the contribution to Venus seismo-acoustic coupling would arise from the dynamics of the blocks. As a starting point, one could assume that the blocks have no topographic features. The complex block displacement can then be considered a superposition of simple eigen-motions such as piston-like vertical oscillations, rocking, tilting, buckling, sliding, and rotation.

For example, a vertical movement of the entire block can be modeled as a baffled piston. A starting assumption is that the block size is much larger than the emitted acoustic wavelength; hence, the sound energy will be directed upward. Dynamic buckling of the blocks can result in the formation of transient cusps with a dominant vertical component, which can produce acoustic perturbations. Tilting motion will generate a complex wavefield due to the vertical displacement of different block parts [e.g., Shani-Kadmiel *et al.* (2021)]. Motion in the horizontal plane, such as sliding or rotation, will not generate sound vertically; it could, however, couple into surface modes radiating acoustic energy into the atmosphere. In addition, stress relief at the blocks' boundaries can excite surface wave modes, which will be coupled to acoustic motion in the gas.

Another factor that might affect the sound field in the lower atmosphere of Venus is the overall near-surface thermal structure. Thus, boundary layer turbulence, local convective stability, potential temperature profiles, and degree of

mixedness of the deep atmosphere could each play a role, to varying degrees, in the first stages of the acoustic perturbation. Therefore, in future work, the accuracy of the coupling predictions could benefit from estimates and measurements of the thermal heterogeneity of the near-surface atmosphere.

ACKNOWLEDGMENTS

This study has been funded by the Louisiana Space Grant Consortium (LaSPACE). We would like to thank Stephen Arrowsmith for constructive discussions, and the reviewers for their much-appreciated comments.

APPENDIX A: IMPLEMENTING THE P-R EOS IN THE ATMOSPHERIC WAVENUMBER MODEL

The adiabatic sound speed c_0 and attenuation coefficient α_0 are obtained from the real and, respectively, imaginary part of the effective (complex-valued and frequency-dependent) wavenumber \tilde{k} . They have a frequency dependence arising from both classical (thermo-viscous) and non-classical (mostly vibrational) processes. The effective wavenumber is

$$\tilde{k}(\omega) = \omega \sqrt{\frac{M}{-\left(\frac{\partial p}{\partial v}\right)_T \tilde{\gamma}(\omega) v^2}} \stackrel{!}{=} \frac{\omega}{c_0(\omega)} + i\alpha_0(\omega). \tag{A1}$$

$v = M\rho^{-1}$ is the molar volume and M the molecular weight. The tilde denotes complex quantities. $\tilde{\gamma} \equiv \tilde{c}_p/\tilde{c}_v$ is the isobaric-to-isochoric ratio of effective molar heat capacities $\tilde{c}_{p(v)} \equiv c_{p(v)}^{\text{ext}} + \sum_n c_n^{\text{int}}(1 - i\omega\tau_n)^{-1}$, where $c_{p(v)}^{\text{ext}}$ are associated with the external (i.e., translational) degrees of freedom while c_n^{int} and τ_n represent the heat capacity and relaxation time, respectively, of the n -th internal (mostly vibrational) molecular degree of freedom (Herzfeld and Litovitz, 1959). The speed of sound and attenuation coefficient are obtained from Eq. (A1),

$$c_0(\omega) = \frac{\omega}{\text{Re}\tilde{k}} = -\frac{v^2}{M} \left(\frac{\partial p}{\partial v}\right)_T \sqrt{\frac{2|\tilde{\gamma}|}{1 + \text{Re}\tilde{\gamma}}}, \tag{A2}$$

$$\alpha_0(\omega) = \text{Im}\tilde{k} = \omega \frac{M}{v^2} \left(\frac{\partial p}{\partial v}\right)_T^{-1} \sqrt{\frac{1 - \text{Re}\tilde{\gamma}}{2|\tilde{\gamma}|}}. \tag{A3}$$

The external heat capacities for a real gas are calculated as corrections to their ideal-gas counterparts as

$$c_p^{\text{ext}} = c_p^0 - R_0 - T \frac{\left(\frac{\partial p}{\partial T}\right)_v^2}{\left(\frac{\partial p}{\partial v}\right)_T} + T \int_{\infty}^v \left(\frac{\partial^2 p}{\partial T^2}\right)_v dv, \tag{A4}$$

$$c_v^{\text{ext}} = c_p^{\text{ext}} + T \frac{\left(\frac{\partial p}{\partial T}\right)_v^2}{\left(\frac{\partial p}{\partial v}\right)_T}, \tag{A5}$$

where c_p^0 is the ideal-gas isobaric molar heat capacity. The P-R EoS can be written as

$$p(v, T) = \frac{R_0 T}{v - b} - \frac{\Theta(T)}{G(v; b)} \tag{A6}$$

or as a cubic equation in the compressibility $Z \equiv pv/R_0T$,

$$Z^3 + (B - 1)Z^2 + (A - 2B - 3B^2)Z - (AB - B^2 - B^3) = 0. \tag{A7}$$

$R_0 = 8.314 \text{ J K}^{-1} \text{ mol}^{-1}$ is the universal gas constant and b the exclusion volume. The functions in the second term on the right-hand side are $G(v; b) \equiv v^2 + 2bv - b^2$ and $\Theta(T) \equiv a [1 + f(\varpi) (1 - \sqrt{T_r})]^2$ where $f(\varpi) \equiv 0.37464 + 1.54226\varpi - 0.2699\varpi^2$ contains the dependence on the acentric factor ϖ . In Eq. (A7), $A = p\Theta/R_0^2T^2$ and $B = bp/R_0T$. Equation (A6) yields the partial derivatives for the heat capacities in Eq. (A4):

$$\left(\frac{\partial p}{\partial T}\right)_v = \frac{R_0}{v - b} + \frac{af(\varpi) [1 + f(\varpi) (1 - \sqrt{T_r})]}{\sqrt{T_r} G(v; b)}, \tag{A8}$$

$$\left(\frac{\partial p}{\partial v}\right)_T = -\frac{R_0 T}{(v - b)^2} + \frac{2(v + b)a [1 + f(\varpi) (1 - \sqrt{T_r})]^2}{G^2(v; b)}, \tag{A9}$$

$$\left(\frac{\partial^2 p}{\partial T^2}\right)_v = -\frac{af(\varpi)}{2G(v; b) T T_c} \times \left[f(\varpi) + \frac{1 + f(\varpi) (1 - \sqrt{T_r})}{\sqrt{T_r}} \right], \tag{A10}$$

$$T \int_{\infty}^v \left(\frac{\partial^2 p}{\partial T^2}\right)_v dv = -\frac{af(\varpi)}{T_c} I(v, b) \times \left[f(\varpi) + \frac{1 + f(\varpi) (1 - \sqrt{T_r})}{\sqrt{T_r}} \right], \tag{A11}$$

where $I(v, b) \equiv \int_{\infty}^v G(v, b)^{-1} dv = [2b\sqrt{(2)}]^{-1} \{ \ln [v + b(1 - \sqrt{2})] - \ln [v + b(1 + \sqrt{2})] \}$. Equation (A7) yields three solutions for Z of which the smallest corresponds to the liquid phase density and the largest to the gas-phase density ρ_0 (of interest here).

APPENDIX B: PLANE-WAVE REFLECTION AND TRANSMISSION COEFFICIENTS

The incidence and reflection angles in the solid are θ_L and θ_T , respectively, for longitudinal and transverse waves; the transmission angle of longitudinal waves in the gas is θ_0 . It is assumed that only longitudinal modes propagate in the atmosphere. The plane wave intensity coefficients for solid-to-gas energy transfer are obtained as follows (Ergin, 1952):

$$\begin{aligned}
 \mathcal{R}_{LL} &= |\mathcal{R}_{LL}|^2, & \mathcal{R}_{LT} &= \frac{c_L}{c_T} \frac{\cos \theta_T}{\cos \theta_L} |\mathcal{R}_{LT}|^2, \\
 \mathcal{R}_{TT} &= |\mathcal{R}_{TT}|^2, & \mathcal{R}_{TL} &= \frac{c_T}{c_L} \frac{\cos \theta_L}{\cos \theta_T} |\mathcal{R}_{TL}|^2, \\
 \mathcal{T}_{LL} &= \frac{\rho_0 c_0^{-1}}{\rho_1 c_L^{-1}} \frac{\cos \theta_0}{\cos \theta_L} |\mathcal{T}_{LL}|^2, \\
 \mathcal{T}_{TL} &= \frac{\rho_0 c_0^{-1}}{\rho_1 c_T^{-1}} \frac{\cos \theta_0}{\cos \theta_T} |\mathcal{T}_{TL}|^2.
 \end{aligned} \tag{B1}$$

The phase speeds and angles of incidence, reflection, and transmission are related via Snell’s second law $c_0/\sin \theta_0 = c_L/\sin \theta_L = c_T/\sin \theta_T$ or, equivalently, $k_0 \sin \theta_0 = k_L \sin \theta_L = k_T \sin \theta_T$, where k_i ($i = 0, L, T$) are the wavenumbers. The quantities \mathcal{R}_{LL} , \mathcal{R}_{LT} , \mathcal{R}_{TL} , \mathcal{R}_{TT} , \mathcal{T}_{LL} , and \mathcal{T}_{TL} represent the amplitude reflection and transmission coefficients, obtained as ratios of displacement potentials ψ_L and ψ_T , defined such that the P - and S -wave displacements are, respectively, $\mathbf{u}_L \equiv \nabla \psi_L$ and $\mathbf{u}_T \equiv \nabla \times \psi_T$. The reflection and transmission coefficients for the displacement potentials ψ at the crust-atmosphere interface are given below, based on Chap. 4 of Brekhovskikh and Godin (1998),

$$\begin{aligned}
 \mathcal{R}_{LL} &:= \frac{\psi_L^{\text{refl}}}{\psi_L^{\text{inc}}} = \frac{Z_0 + Z_T \sin^2 2\theta_T - Z_L \cos^2 2\theta_T}{Z_0 + Z_T \sin^2 2\theta_T + Z_L \cos^2 2\theta_T}, \\
 \mathcal{R}_{LT} &:= \frac{\psi_T^{\text{refl}}}{\psi_L^{\text{inc}}} = -\frac{2(1 - \mathcal{R}_{LL}) \cot \theta_L \sin^2 \theta_T}{\cos 2\theta_T}, \\
 \mathcal{R}_{TT} &:= \frac{\psi_T^{\text{refl}}}{\psi_T^{\text{inc}}} = -\frac{Z_0 + Z_L \cos^2 2\theta_T - Z_T \sin^2 2\theta_T}{Z_0 + Z_L \cos^2 2\theta_T + Z_T \sin^2 2\theta_T}, \\
 \mathcal{R}_{TL} &:= \frac{\psi_L^{\text{refl}}}{\psi_T^{\text{inc}}} = \frac{(1 + \mathcal{R}_{TT}) \tan \theta_L \cos 2\theta_T}{2 \sin^2 \theta_T}, \\
 \mathcal{T}_{LL} &:= \frac{\psi_L^{\text{tran}}}{\psi_L^{\text{inc}}} = \frac{(1 - \mathcal{R}_{LL}) \tan \theta_0 \cot \theta_L}{\cos 2\theta_T}, \\
 \mathcal{T}_{TL} &:= \frac{\psi_L^{\text{tran}}}{\psi_T^{\text{inc}}} = \frac{(1 + \mathcal{R}_{TT}) \tan \theta_0}{2 \sin^2 \theta_T}.
 \end{aligned} \tag{B2}$$

The first subscript indicates the incident mode; the second subscript denotes the reflected or transmitted mode. The coefficients are expressed in terms of the angle-dependent characteristic acoustic impedances of the atmosphere (Z_0) and the crust (Z_L and Z_T for longitudinal and transverse waves, respectively). For plane waves, these are $Z_0 = \rho_0 c_0 / \cos \theta_0$, $Z_L = \rho_1 c_L / \cos \theta_L$ and $Z_T = \rho_1 c_T / \cos \theta_T$.

APPENDIX C: POWER TRANSMITTED ACROSS A SOLID-GAS INTERFACE FROM AN OMNIDIRECTIONAL P -WAVE SOURCE

A monopole source located at $z = -z_s$ produces spherical waves at \mathbf{r} . Since this field will be incident on a planar interface at $z = 0$, it is useful to decompose it in elementary plane waves via a Weyl integral (Williams, 1999),

$$\begin{aligned}
 \frac{p(\mathbf{r})}{p_0 r_0} &= \frac{\exp(ik|\mathbf{r} + z_s \hat{\mathbf{z}}|)}{|\mathbf{r} + z_s \hat{\mathbf{z}}|} \\
 &= \frac{i}{2\pi} \int_{-\infty}^{+\infty} dk_x \int_{-\infty}^{+\infty} dk_y e^{i(k_x x + k_y y)} \frac{e^{ik_z |z + z_s|}}{k_z},
 \end{aligned} \tag{C1}$$

where p_0 , r_0 are arbitrary reference values. In the presence of the interface at $z = 0$, in order to find the acoustic field coupled from a P -wave generated in the solid ($z < 0$) into a P -wave in the gas ($z > 0$), Eq. (C1) must be modified to account for sound transmitted across the interface. Since the pressure in a plane harmonic wave can be expressed as $p = \rho \omega^2 \psi$, then the transmission coefficient for the pressure amplitude is $\mathcal{T}_{LL}^{(p)} = m \mathcal{T}_{LL}$, where $m = \rho_0 / \rho_1$ and the displacement-amplitude coefficient $\mathcal{T}_{LL}(q)$ is calculated from Eqs. (B2). Introducing the horizontal wave-vector $\mathbf{q} \equiv (k_x, k_y, 0)$ and the vertical wavenumber $\nu \equiv k_z$, one obtains (Godin, 2011; McDonald and Calvo, 2007)

$$\frac{p(\mathbf{r})}{p_0 r_0} = \frac{m}{2\pi^2} \iint d^2 \mathbf{q} F(\mathbf{q}, z) e^{i\mathbf{q} \cdot \mathbf{r}}, \tag{C2}$$

where $F(\mathbf{q}, z) = i\pi [\mathcal{T}_{LL}(q) / \nu_L(q)] e^{i[\nu_L(q)z_s - \nu_0(q)z]}$ and $\nu_L = (k_L^2 - q^2)^{1/2}$ and $\nu_0 = (k_0^2 - q^2)^{1/2}$ are the vertical wavenumbers in the crust and atmosphere, respectively, with $k_0 = \omega / c_0$. The acoustic power transmitted into the atmosphere is obtained by integrating the z component of the Poynting vector (intensity) over the infinite interface in the xy plane and using plane wave orthonormality, i.e., $\iint d\mathbf{r} \exp[i(\mathbf{q}' - \mathbf{q}) \cdot \mathbf{r}] = (2\pi)^2 \delta(\mathbf{q}' - \mathbf{q})$:

$$\begin{aligned}
 \Pi_{\text{atm}} &= \iint_{(z=0)} \mathbf{S}_{\text{avg}} \cdot \hat{\mathbf{z}} dA \\
 &= \frac{1}{2\rho_0 \omega} \int_{-\infty}^{+\infty} \int_{-\infty}^{+\infty} \text{Im} \left[p^*(\mathbf{r}) \frac{\partial p(\mathbf{r})}{\partial z} \right]_{z=0} dx dy \\
 &= (p_0 r_0)^2 \frac{m^2}{2\pi^2 \rho_0 \omega} \iint \text{Im} \left[F^* \frac{\partial F}{\partial z} \right]_{z=0} d^2 \mathbf{q} \\
 &= (p_0 r_0)^2 \frac{m^2}{\pi \rho_0 \omega} \int_0^{\omega/c_0} q \text{Im} \left[F^* \frac{\partial F}{\partial z} \right]_{z=0} dq.
 \end{aligned} \tag{C3}$$

The arbitrariness associated with the reference pressure p_0 and location r_0 is eliminated by normalizing to the total power of P waves emitted in an unbounded solid, $\Pi_{\text{em}} = 2\pi(p_0 r_0)^2 / \rho_1 c_L$, yielding Eq. (1).

Arrowsmith, S., Negraru, P., and Johnson, G. (2021). “Bolide energetics and infrasound propagation: Exploring the 18 December 2018 Bering Sea event to identify limitations of empirical and numerical models,” *Seismic Rec.* **1**(3), 164–171.

Averbuch, G., Assink, J. D., and Evers, L. G. (2020a). “Long-range atmospheric infrasound propagation from subsurface sources,” *J. Acoust. Soc. Am.* **147**(2), 1264–1274.

Averbuch, G., Waxler, R. M., Smets, P. S. M., and Evers, L. G. (2020b). “Probabilistic inversion for submerged source depth and strength from infrasound observations,” *J. Acoust. Soc. Am.* **147**(2), 1066–1077.

Bowman, D. C., Rouse, J. W., Krishnamoorthy, S., and Silber, E. A. (2022). “Infrasound direction of arrival determination using a balloon-borne aeroseismometer,” *JASA Express Lett.* **2**(5), 054001.

Brekhovskikh, L. M., and Godin, O. (1998). *Acoustics of Layered Media* (Springer-Verlag, Berlin).

- Brissaud, Q., Krishnamoorthy, S., Jackson, J. M., Bowman, D. C., Komjathy, A., Cutts, J. A., Zhan, Z., Pauken, M. T., Izraelevitz, J. S., and Walsh, G. J. (2021). "The first detection of an earthquake from a balloon using its acoustic signature," *Geophys. Res. Lett.* **48**(12), e2021GL093013, <https://doi.org/10.1029/2021GL093013>.
- Byrne, P. K., Ghail, R. C., Gilmore, M. S., Şengör, A. C., Klimczak, C., Senske, D. A., Whitten, J. L., Khawja, S., Ernst, R. E., and Solomon, S. C. (2021). "Venus tesserae feature layered, folded, and eroded rocks," *Geology* **49**(1), 81–85.
- Byrne, P. K., Ghail, R. C., Şengör, A. M. C., James, P. B., Klimczak, C., and Solomon, S. C. (2018). "A globally fragmented and mobile lithosphere on Venus," in *16th Meeting of the Venus Exploration and Analysis Group (VEXAG)*, Vol. 16, p. 8008.
- Byrne, P. K., Ghail, R. C., Şengör, A. M. C., Klimczak, C., and Solomon, S. C. (2017). "Lateral motion of crustal blocks has been widespread on Venus," in *Lunar and Planetary Science Conference*, p. 2708.
- Byrne, P. K., and Krishnamoorthy, S. (2022). "Estimates on the frequency of volcanic eruptions on Venus," *JGR Planets* **127**(1), e2021JE007040.
- Ergin, K. (1952). "Energy ratio of the seismic waves reflected and refracted at a rock-water boundary," *Bull. Seismol. Soc. Am.* **42**, 349–372.
- Evers, L. G., and Haak, H. W. (2010). "The characteristics of infrasound, its propagation and some early history," *Infrasound Monit. Atmos. Stud.* 3–27.
- Ewing, W. M., Jardetzky, W. S., Press, F., and Beiser, A. (1957). *Elastic Waves in Layered Media* (McGraw Hill, New York).
- Garcia, R., Lognonné, P., and Bonnin, X. (2005). "Detecting atmospheric perturbations produced by Venus quakes," *Geophys. Res. Lett.* **32**, L16205, <https://doi.org/10.1029/2005GL023558>.
- Godin, O. A. (2011). "Low-frequency sound transmission through a gas-solid interface," *J. Acoust. Soc. Am.* **129**(2), EL45–EL51.
- Herzfeld, K. F., and Litovitz, T. H. (1959). *Absorption and Dispersion of Ultrasonic Waves* (Academic Press, New York), Chap. II, Secs. 20 and 21.
- Jensen, F. B., Kuperman, W. A., Porter, M. B., and Schmidt, H. (2011). *Computational Ocean Acoustics* (Springer New York, New York).
- Johnston, D. H., Toksöz, M. N., and Timur, A. (1979). "Attenuation of seismic waves in dry and saturated rocks: II. Mechanisms," *Geophysics* **44**(4), 691–711.
- Krishnamoorthy, S., Lai, V. H., Komjathy, A., Pauken, M. T., Cutts, J. A., Garcia, R. F., Mimoun, D., Jackson, J. M., Bowman, D. C., Kassarian, E., Martire, L., Sournac, A., and Cadu, A. (2019). "Aerial seismology using balloon-based barometers," *IEEE Trans. Geosci. Remote Sens.* **57**(12), 10191–10201.
- Lebonnois, S., and Schubert, G. (2017). "The deep atmosphere of Venus and the possible role of density-driven separation of CO₂ and N₂," *Nat. Geosci.* **10**, 473–477.
- Leftwich, T. E., von Frese, R. R. B., Kim, H. R., Noltimier, H. C., Potts, L. V., Roman, D. R., and Tan, L. (1999). "Crustal analysis of Venus from Magellan satellite observations at Atalanta Planitia, Beta Regio, and Thetis Regio," *J. Geophys. Res.* **104**(E4), 8441–8462, <https://doi.org/10.1029/1999JE900007>.
- Madariaga, R. (2015). "Seismic source theory," in *Treatise on Geophysics* (Elsevier, Amsterdam), pp. 51–71.
- McDonald, B. E., and Calvo, D. C. (2007). "Enhanced sound transmission from water to air at low frequencies," *J. Acoust. Soc. Am.* **122**(6), 3159–3161.
- Morellina, S., and Bellan, J. (2022). "Turbulent chemical-species mixing in the Venus lower atmosphere at different altitudes: A direct numerical simulation study relevant to understanding species spatial distribution," *Icarus* **371**, 114686.
- Morellina, S., Bellan, J., and Cutts, J. (2020). "Global thermodynamic, transport-property and dynamic characteristics of the Venus lower atmosphere below the cloud layer," *Icarus* **350**, 113761.
- Petculescu, A. (2016). "Acoustic properties in the low and middle atmospheres of Mars and Venus," *J. Acoust. Soc. Am.* **140**(2), 1439–1446.
- Petculescu, A., and Achi, P. (2012). "A model for the vertical sound speed and absorption profiles in Titan's atmosphere based on Cassini-Huygens data," *J. Acoust. Soc. Am.* **131**, 3671–3679.
- Petculescu, A., and Lueptow, R. M. (2007). "Atmospheric acoustics of Titan, Mars, Venus, and Earth," *Icarus* **186**(2), 413–419.
- Pettengill, G., and Price, R. (1961). "Radar echoes from Venus and a new determination of the solar parallax," *Planet. Space Sci.* **5**(1), 71–74.
- Shani-Kadmiel, S., Averbuch, G., Smets, P., Assink, J., and Evers, L. (2021). "The 2010 Haiti earthquake revisited: An acoustic intensity map from remote atmospheric infrasound observations," *Earth Planet. Sci. Lett.* **560**, 116795.
- Smith, W. B. (1963). "Radar observations of Venus, 1961 and 1959," *Astronom. J.* **68**(1), 15–21.
- Solomon, S. C., Head, J. W., Kaula, W. M., McKenzie, D., Parsons, B., Phillips, R. J., Schubert, G., and Talwani, M. (1991). "Venus tectonics: Initial analysis from Magellan," *Science* **252**(5003), 297–312.
- Taylor, S. R., and McLennan, S. (2008). "Venus: A twin planet to Earth?," in *Cambridge Planetary Science* (Cambridge University, Cambridge), pp. 181–206.
- Trahan, A. J., and Petculescu, A. (2020). "Absorption of infrasound in the lower and middle clouds of Venus," *J. Acoust. Soc. Am.* **148**(1), 141–152.
- Victor, W. K., and Stevens, R. (1961). "Exploration of Venus by radar," *Science* **134**(3471), 46–48.
- Waxler, R., Assink, J., and Velea, D. (2017). "Modal expansions for infrasound propagation and their implications for ground-to-ground propagation," *J. Acoust. Soc. Am.* **141**(2), 1290–1307.
- Williams, E. G. (1999). *Fourier Acoustics* (Academic Press, London), Chap. 2.
- Xiao, C., Li, F., Yan, J., Gregoire, M., Hao, W., Harada, Y., Ye, M., and Barriot, J.-P. (2021). "Possible deep structure and composition of Venus with respect to the current knowledge from geodetic data," *JGR Planets* **126**(7), e2019JE006243, <https://doi.org/10.1029/2019JE006243>.
- Yang, A., Huang, J., and Wei, D. (2016). "Separation of dynamic and isostatic components of the Venusian gravity and topography and determination of the crustal thickness of Venus," *Planet. Space Sci.* **129**, 24–31.
- Yoder, C. F. (1995). "Venus' free obliquity," *Icarus* **117**(2), 250–286.
- Zuber, M. T. (1987). "Constraints on the lithospheric structure of Venus from mechanical models and tectonic surface features," *J. Geophys. Res.* **92**, E541–E551, <https://doi.org/10.1029/JB092iB04p0E541>.